# TENSILE TESTING OF PINNED HYBRID CFRP/TITANIUM SINGLE-LAP SHEAR JOINTS AND DAMAGE MONITORING WITH ELECTRICAL RESISTANCE MEASUREMENTS

## A. Dengg[1*], C. Kralovec[1], M. Schagerl[1]

[1]Institute of Structural Lightweight Design, Johannes Kepler University,
Altenberger Strasse 69, 4040 Linz, Austria
* andreas.dengg@jku.com

**Keywords:** structural health monitoring, pinned hybrid joint, electrical resistance measurement, single-lap shear

**Summary:** *This contribution presents a new evaluation approach for Structural Health Monitoring of a pinned hybrid CFRP/titanium single-lap shear joint with the help of direct current electrical resistance measurements. The result is a dimensionless, load-independent damage indicator that is similar to an already developed evaluation approach by the authors but is simpler and more robust in comparison. Readily published test data is re-evaluated with the new evaluation approach and compared with the existing structural as well as the electrical resistance results. Finally, further test setup improvements for future tests are discussed.*

## 1  INTRODUCTION

Lightweight design is a critical aspect of civil aircraft manufacturing and operation. Continuous efforts to develop lighter and more fuel-efficient aircraft has led to advances in materials and manufacturing techniques. In particular, pinned hybrid (i.e., multi-material) joints have the potential to gain importance for future aircraft design. Compared to conventional joints, pinned hybrid joints allow the integration of different materials without the weight penalty of fasteners like rivets and bolts. Pinned hybrid joints feature an array of metallic pins that penetrate a fiber-reinforced polymer (FRP). Together with the adhesive properties of the FRP's matrix material, this combination ensures force transfer across the joint [1]. Conventional adhesive joints are also used in aircraft construction, but proper surface preparation is elaborate and costly, and obtainable joint strength as well as damage tolerance is comparatively low. Pinned hybrid joints offer promising properties in terms of damage tolerance, weight reduction and joint strength [2]. For these reasons, the study of the dominant damage modes and Structural Health Monitoring (SHM) of pinned hybrid joints is of interest. SHM refers to the process of continuously monitoring and assessing the condition of an aircraft's structure to ensure its safety. For the different levels of SHM, it involves using various physical properties sensitive to damage and associated sensors to detect (level 1), locate (level 2), quantify (level 3) and typify (level 4) any potential damage [3].

The authors' current research investigates a pinned hybrid joint in the form of a single-lap shear (SLS) geometry, comprised of titanium and epoxy resin based carbon FRP (CFRP) adherends. On the surface of the titanium adherend, additively manufactured titanium pins are created that penetrate the CFRP material as described above. Through literature and structural investigations at the authors' laboratory, cracks at the overlap ends were identified as the dominant damage mode of the considered pinned hybrid SLS joint. Although matrix-related

damage like this is usually investigated by AC ERM methods, the much simpler DC ERM is suitable for this configuration, since the contact of the metallic pins with the carbon fibers creates an electrical conductivity across the overlap (which is not the case with pure adhesive joints, so AC ERM methods are more suitable there). That way, a non-reversible resistance change is associated with damage [4].

However, despite being a simple method, measuring conditions in real-life application are challenging. For the CFRP material as well as the overlap, a piezoresistive behavior is given that challenges the identification of a damage related resistance change. However, in a publication by the authors currently under review, the separation of piezoresistive and non-reversible resistance change of the overlap for damage evaluation is successfully demonstrated [5]. Although successful, the evaluation is extensive and uses strain data obtained by digital image correlation (DIC) which is not convenient for operational applications. In general, a more robust setup and simple data processing is needed with the aim of alleviating internal influences (e.g., piezoresistivity and measurement chain) and external influences (e.g., environmental) of the DC ERM method.

In this research contribution, a new DC ERM damage evaluation approach is proposed which is based on recent results at the author's research group [5], but allows for simpler data processing and more robust and load-independent damage evaluation by including a reference measurement. This results in a dimensionless damage indicator and improved inferences about the condition of the specimen during mechanical loading, including the actual portion of the piezoresistive influence. Differences to the previous evaluation approach developed in [5] and the potential advantages of the novel method are outlined and discussed. Further, an improved instrumentation setup for future tests under high cycle fatigue loading is presented and discussed.

The current contribution is structured as follows. First, the specimen, the structural test setup and its procedure are described. Second, a short description of the methods used in [5] to assess the overlap damage initiation and propagation using DIC is given. Third, the proposed, simple DC ERM evaluation method using the electrical resistance ratio as measure for overlap damage is presented. Afterwards, the results of the investigation are shown: Identified damage initiation and propagation using DIC is presented and together with the electrical resistance ratio for damage evaluation, the new findings are compared and discussed regarding the previous evaluation method. Finally, resulting improvements by the presented method for future experiments are discussed over the existing setup. At the end, conclusions and outlook are found.

## 2 MATERIALS AND METHODS

In this section, the specimen, the test setup, the structural test procedure and the method of determination of damage initiation and propagation with the help of DIC are introduced. Furthermore, the novel, simpler and load-independent DC ERM method for damage evaluation is presented.

### 2.1 Specimen description

The specimen geometry is based on the standard ASTM D-5868 [6] and is comprised of a titanium and CFRP adherend, shown at the left in Figure 1. Each adherend is 101.6 mm long and both adherends overlap for 25.4 mm. At the Ti-6Al-4V titanium adherend, 27 pins are additively manufactured on a 1.7 mm thick titanium strip. There are six pin rows, where each pin is 1.8 mm high, shaped cylindrically (diameter = 0.5) with a tapered end. The 2 mm thick CFRP adherend is created using a layup of six carbon fiber fabrics (5-harness satin weave),

pre-impregnated with an epoxy resin [7]. During the hand layup process, the pins are incorporated into the fabric. Subsequent autoclave curing and cutting to 20 mm width with a diamond saw blade result in the final specimens. For testing, bonded clamping tabs made of glass FRP (GFRP) enable symmetrical clamping inside the test rig and provide electrical insulation for DC ERM. In total, four electrical contacts are created. At the titanium adherend, a wire is connected to the clean, bare metal with electrically conducting silver epoxy (EPO-TEK© H20E, supplied by Epoxy Technology). The top side of the CFRP adherend is etched with sulfuric acid and two lateral surfaces are engraved with a laser to expose the carbon fibers [8]. Wires are connected at these locations with the same silver epoxy. For DIC images, the lateral side of the overlap is covered with a high-contrast, random speckle pattern. At the right in Figure 1, the assumed equivalent circuit diagram is shown, where resistance $R_1$ represents the CFRP adherend's bulk material and $R_2$ represents the resistance of the overlap.
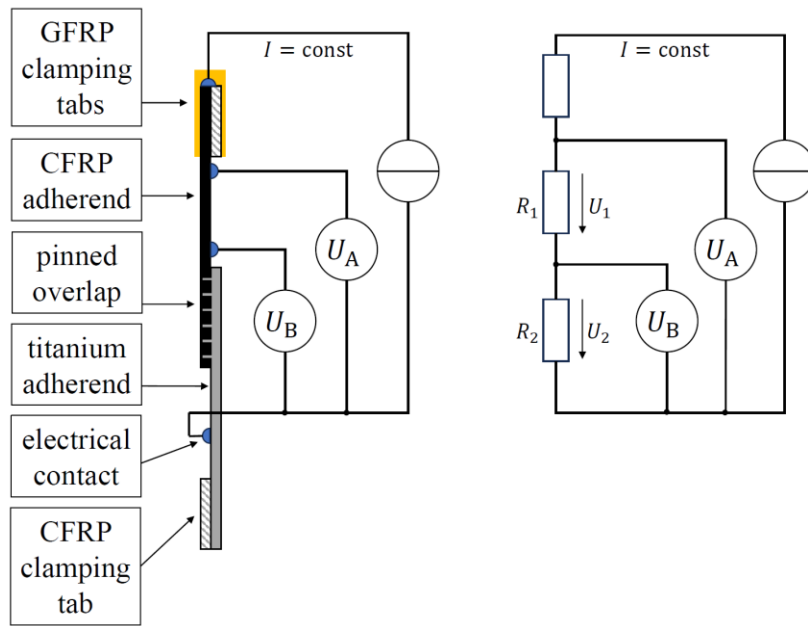
Figure 1: Specimen geometry with electrical measurement setup (left) and simplified equivalent circuit diagram (right).

## 2.2    Test setup and procedure

The setup with the clamped specimen at the test rig is shown in Figure 2. The specimen is subjected to multiple, quasi-static, tension-tension load cycles (0.2 mm/min) with increasing maximum load $F_{max}$. The loading was realized on a test rig equipped with a servo-hydraulic cylinder (25 kN Zwick Roell). Each time, the specimen is unloaded to $F_{min} = 350$ N. After three cycles, the maximum load is increased. The procedure is repeated until specimen failure. During the load cycles, a constant current of 10 mA is introduced (Keithley 6220 precision current source) between the hybrid SLS specimen's top and bottom electrodes. The test rig's load signal and two electrical potentials $U_A$ and $U_B$ are recorded with a data acquisition system at a sampling rate of 300 Hz (HBM QuantumX MX840A). The locations of current introduction and both electrical potential measurements are shown in on the left in Figure 1. A digital camera (Canon EOS 1200D) records images for DIC every second.
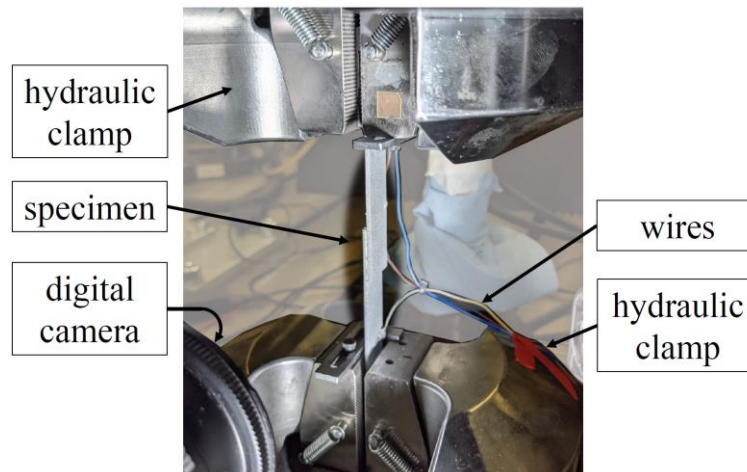
Figure 2: Test rig setup with clamped specimen

## 2.3   Damage initiation and propagation monitoring by DIC

Damage initiation at the overlap ends and damage propagation is determined with the help of DIC, a non-invasive, optical measuring method for evaluating displacements of a specimen's surface [9]. The DIC-observed surface is he lateral side of the overlap. Two DIC-based damage evaluation method are applied.

For the first method, the tangential stiffness across the overlap is determined for every cycle, evaluated at a low load range by averaging between 1.2 and 2.2 kN. The definition of tangential stiffness $k_{\tan}$ as a function of load $F$ and damage $D$ is found in Equation (1). This procedure is presented, experimentally demonstrated and validated using FE analysis in [5] and shows the course of the structural degradation of the overlap. It uses a defined length $L$ that spans across the overlap and evaluates its change as the test progresses.

$$k_{\tan}(D) = \frac{\partial F}{\partial L} \tag{1}$$

For the second method, a criterion for presence of damage using the "spatial one-standard correlation confidence" (also called "correlation confidence", Vic-2D output variable sigma in pixel [10]) is defined. During DIC evaluation, the correlation confidence is estimated on the basis of the gray level correlation standard deviation of each pixel subset. A low standard deviation indicates a high confidence in the spatial correlation of the subsets and vice versa [9]. The recorded speckle pattern is influenced by everything that changes the gray values of the subsets, such as a displacement of the specimen, changes of illumination conditions and damage to the speckle pattern. That way, by assuming constant experimental conditions, damage to the speckle pattern (bonded to the specimen surface) has a dominant influence on the correlation confidence value, since all other influences are lower or kept constant. Thus, a threshold value of correlation confidence can be defined to indicate the presence of a crack. In the presented results, this threshold value is defined and validated by the ultimate crack lengths at the overlap ends, measured separately at the post-test fraction surfaces of the specimen. With a threshold value determined this way, it is possible to identify the location and time of occurrence of damage at the respective overlap ends, as well as crack length determination. This process and all its results are described in detail in [5].

4

## 2.4 Damage indicator for load-independent overlap damage evaluation

To show that the overlap damage is accompanied by a non-reversible change in resistance, the specimen is modelled with two electrical resistances in series. The simplified electrical circuit of the specimen is shown in Figure 1, where $R_1$ spans across the bulk material of the CFRP adherend and $R_2$ spans across the overlap. The same constant current $I$ flows through both resistances. The resistances are assumed to be temperature independent (for the performed measurements under laboratory conditions) and linear piezoresistive. The latter is also supported by previous results [5].

Considering the specimen to damage at the joint overlap, the ratio of the two resistances can be used for damage monitoring. According to [5], the resistances can be well described by a linear strain-dependent term, thus, can be approximated by

$$\frac{R_2}{R_1} \approx \frac{R_2^0(1+\text{GF}_2\varepsilon_2)+R_2^d(\varepsilon,D)}{R_1^0(1+GF_1\varepsilon_1)}, \tag{2}$$

where the linear piezoresistive behavior of each resistance is modeled with initial resistance $R^0$, an individual gauge factor GF and strain $\varepsilon$ [11]. Damage in the bulk material of the CFRP adherend is not expected, thus, no non-reversible increase in resistance is expected for $R_1$. However, the opposite is the case for $R_2$, where the non-reversible resistance term $R_2^d(\varepsilon, D)$ is considered dependent on strain $\varepsilon$ and damage state $D$. This portion $R_2^d(\varepsilon, D)$ starts at zero for no damage and increases, as damage initiates and propagates.

However, the actual resistance ratio of the test setup is measured by

$$\frac{R_2}{R_1} = \frac{U_2 I}{U_1 I} = \frac{U_\text{B}}{U_\text{A}-U_\text{B}}, \tag{3}$$

where the electrical current $I$ can be eliminated in Equation (3). Consequently, the measured potential $U_2$ has the same linear dependency on strain as the resistances (cf., Equation (2)), and thus, can be used and further fitted for an unchanged damage state by the linear function

$$f = kU_1 + d, \tag{4}$$

where $k$ and $d$ are the linear fit parameters found from DC ERM data. That way, a function $f$ is available for every load cycle $i$, that reflects the joint's piezoresistive behavior as a function of $U_1$.

Consequently, a load independent damage indicator can be defined that evaluates the difference between a measured $U_2$ value and a value predicted by the fit function for the pristine state with the simultaneously measured $U_1$ value. A mean behavior for the pristine specimen's overlap's strain dependent electrical potential $\overline{U}_2^p$ can be determined by averaging the fit functions $f$ of $n$ load cycles measured in pristine condition. Thus, the proposed damage indicator is defined by

$$\text{DI} = \frac{1}{U_2^{\text{p},0}} \big[ \underbrace{U_2}_{\substack{\text{measured} \\ \text{potential}}} - \underbrace{\overline{U}_2^p}_{\substack{\text{approximated} \\ \text{potential of the} \\ \text{pristine overlap}}} \big]. \tag{5}$$

As reference, the electrical potential at the un-strained pristine joint $U_2^{\text{p},0}$ appears meaningful. Results from [5] show that the non-reversible resistance $R_2^d$ of the overlap rises with increasing damage, thus, the proposed DI value indicates damage when it significantly and positively deviates from zero.

## 3    RESULTS AND DISCUSSION

In this section, the results are shown and discussed. First, the structural results are presented, specifically when and where damage occurs at the overlap and what effect it has on the tangential stiffness. Second, the results for the proposed strain independent DI are presented and discussed based on the comparison with the damage indicator presented in [5] and the DIC-based observation of the damage initiation and propagation. Finally, potential improvements for future damage monitoring by DC ERM during cyclic fatigue test campaigns with pinned hybrid SLS joint specimens are discussed.

### 3.1    Results of structural testing and damage initiation

A total of 28 load cycles were performed until specimen failure. The specimen failed at 6.65 kN. The first three load cycles are not considered in the evaluation because the tested load level (lowest load level, $F_{\max} = 1.2$ kN) resulted in poor raw data quality due to friction issues at the test rig. Thus, raw data from cycle no. 4 onwards is used for evaluation. Table 1 lists the load cycles evaluated in this work.

Table 1: Summary of evaluated cycles [5].

| cycle no. during test | 4-6 | 7-9 | 10-12 | 13-15 | 16-18 | 19-21 | 22, 23 | 24-26 | 27, 28 |
|---|---|---|---|---|---|---|---|---|---|
| load level $F_{\max}$ in kN | 2.2 | 3.2 | 3.9 | 4.2 | 4.8 | 5.2 | 5.7 | 6.2 | 7.2 |

According to the DIC-based damage detection, the first damage initiation at the titanium overlap end can be determined at 2.9 kN during cycle no. 7 [5]. Thus, load cycles no. 4 to 6 are used for the determination of the pristine behavior of the electrical potential at the overlap $\bar{U}_2^p$, as described in Section 2.4. The second damage initiation at the CFRP overlap end occurred at 3.6 kN during cycle no. 10. Figure 3 presents the DIC images of the load cycles no. 7 and no. 10 with their spatial correlation confidence and the identified locations of damage initiation.
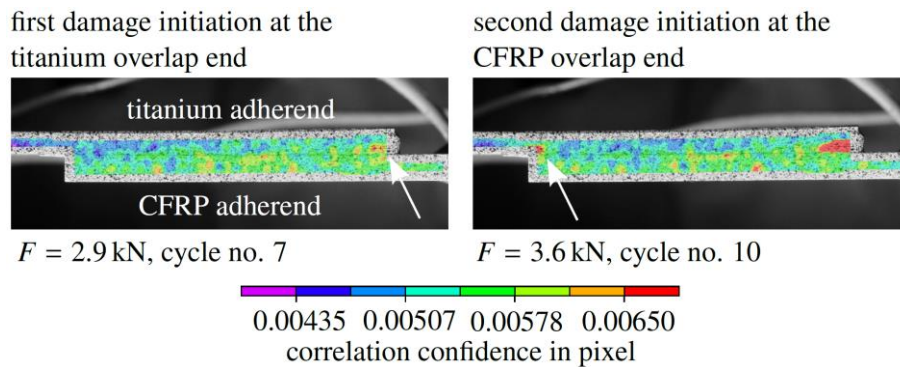


Figure 3: DIC images with spatial correlation confidence and locations of damage initiation [5].

For the structural results, the joint's tangential compliance $c_{\tan} = 1/k_{\tan}$ is chosen for better visualization compared to the tangential stiffness. It is shown in Figure 4 for the respective load cycle, along with the determined crack lengths at both overlap ends. Due to the selected evaluation parameters for the DIC system, no statement about the crack length can be made

6

directly at the free edge of the specimen. This DIC free edge detection limit is approximately 0.8 mm towards the free edge of the overlap and is indicated as well in Figure 4. The changes in the tangential compliance are associated with the progress of the detected crack lengths at the titanium and CFRP overlap end respectively. The tangential compliance remains approximately constant up to the first damage initiation at the CFRP overlap end. It increases slightly from cycle no. 7 onwards. Especially after cycle no. 10, its value increases significantly, which can be attributed to the second damage initiation, which occurs at the titanium overlap end. Following an intermediate decrease after cycle no. 12, the tangential compliance increases monotonically until specimen failure.
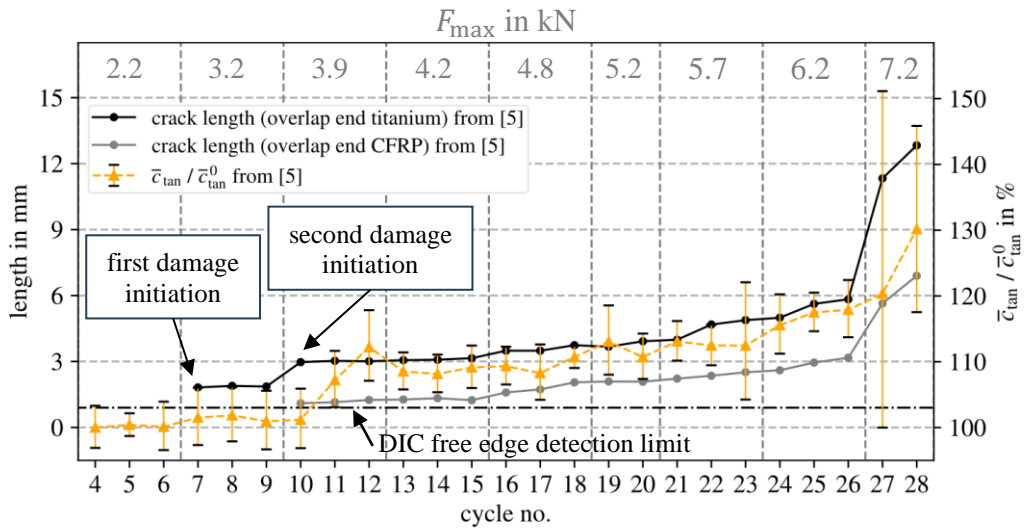


Figure 4: Determined crack lengths of both overlap ends and tangential compliance for the respective load cycle.

## 3.2 Damage indicator results

Raw data of $U_A$ and $U_B$ is filtered (second order Butterworth filter, cutoff frequency $\omega_c = 3$ Hz) and the electrical potentials $U_1 = U_A - U_B$ and $U_2 = U_B$ are calculated (cf., Figure 1). Furthermore, only electrical potentials during loading are used in this study for better comparability with the structural analysis (cf., Section 3.1). Finally, unexplainable jumps were removed from measurement raw data (predominantly for small loading at the load cycles no. 24 to 28). On the left in Figure 5, the filtered data is shown. The different load levels are highlighted by different colors. The data of the single load cycles is still very noisy, however, the linear relation between $U_1$ and $U_2$ is evident. Nevertheless, for better data representation, the found fits of the linear function $f$ and their standard deviations are plotted in Figure 5 right.
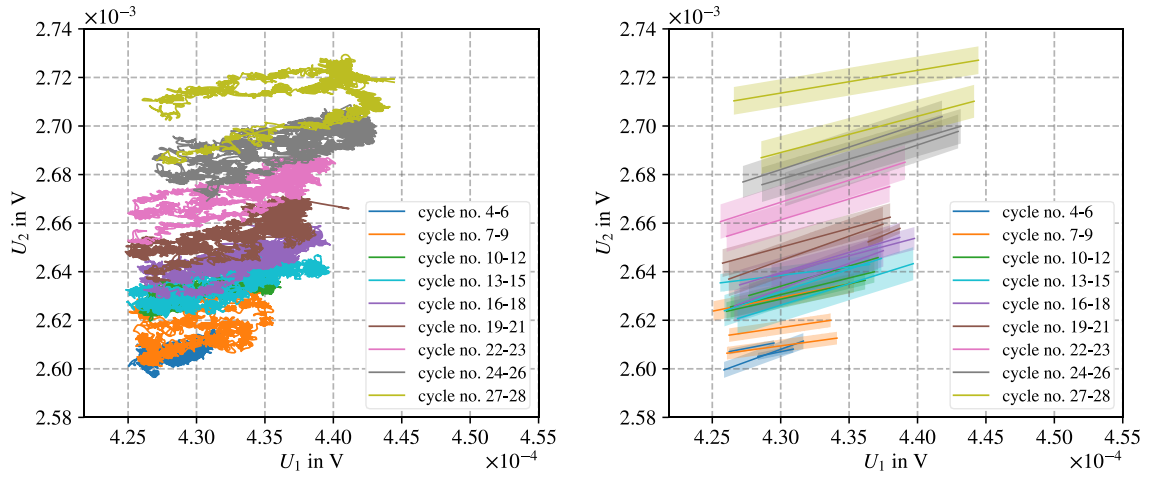
Figure 5: Electrical potential $U_2$ plotted over $U_1$ while structural loading, grouped into the individual load cycles (left) and linear fit results and its standard deviation (transparent range) of each cycle (right).

To further underline the feasibility of the made assumptions, the coefficient of determination (COD) of the found linear fits are calculated. Thereby, also the quality of the raw data of the load cycles can be assessed and raw data with poor quality (i.e., bad COD of linear fit) is easily identified. Furthermore, based on previous results it is assumed, that initiating and propagating damage does not significantly change the piezoresistive behavior of the overlap [5], i.e., the fit parameter $k$. Both the coefficient of determination and the fit parameter $k$ are shown in Figure 6. The vertical lines indicate the different load levels listed in Table 1.
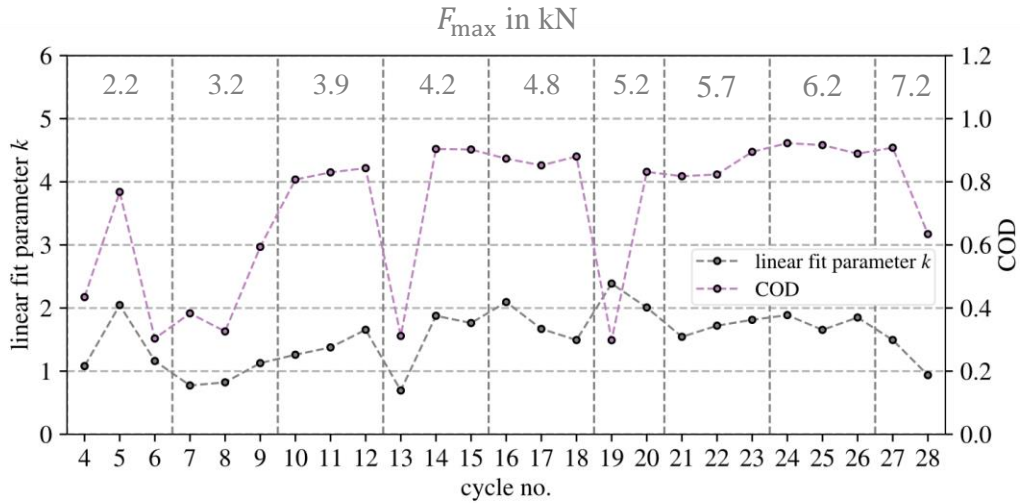


Figure 6: Linear fit parameter $k$ and $COD$ for the respective load cycle.

The COD is generally not very high, indicating that higher order fit functions may be advantageous. However, for the present study, the linear fit is assumed to be adequate, as most COD are in a range of 0.8 to 0.95. Certain load cycles show a COD below 0.7: From these, cycles no. 7, 8, 13 and 28 were also sorted out from evaluation in [5]. The bad correlations with the linear fits are believed to come from the damage progress during these cycles. In the present study, cycles no. 4, 6, 9 and 19 show also low values of COD. For cycles no. 4, 6 and

9, a closer examination of the corresponding data plot of $U_1$ and $U_2$ shows scattering within the dataset. Furthermore, these datasets are smaller than the datasets obtained at higher load levels. This circumstance makes the fit difficult and results in a higher deviation from the linear relationship. For cycle no. 19, little data for $U_1$ and $U_2$ is available due to a measurement issue. Nevertheless, the fit parameter $k$ is overall not subject to a clear tendency to change during test progression and progressing damage, although the particular values vary significantly. To demonstrate the robustness of the presented damage indicator, all found values are used further to calculate the DI value.

The damage indicator is calculated according to Equation (5). First, the linear fit function predicting $\overline{U}_2^p$ with the simultaneously measured $U_1$ value is established. This function is averaged from the linear fits of load cycles no. 4 to 6, where the joint overlap is undamaged (cf. Section 3.1). Second, $U_2^{p,0}$ is calculated by the established linear fit function predicting $\overline{U}_2^p$, by considering the smallest potential measured for $U_1$ in the specimen's pristine condition. This specific value for $U_1$ is chosen, because the potential influence of strain is kept low and it produces a representative baseline value. Third, the filtered data of the electrical potentials $U_1$ and $U_2$ is processed for every load cycle. All recorded potentials from each load cycle are used, without limiting the data to certain strain states. Thus, mean and standard deviation DI values are available for every load cycle, which are shown in Figure 7.
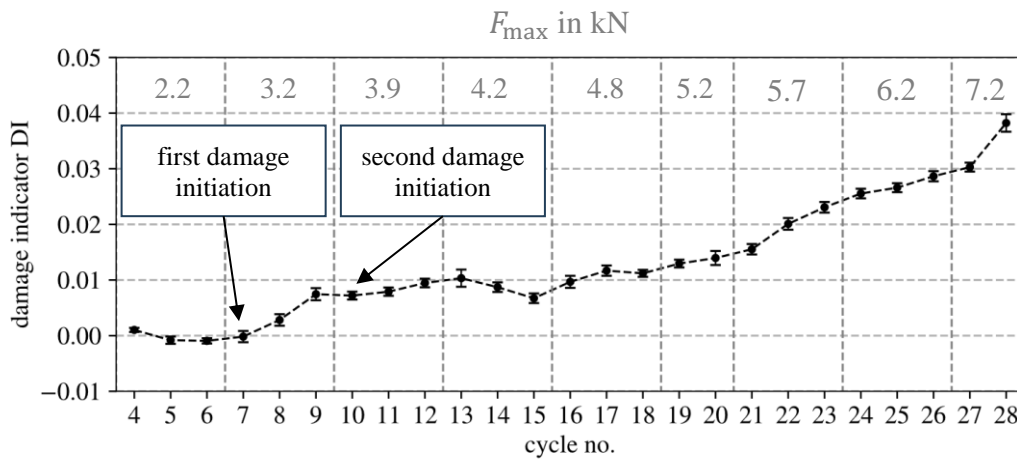


Figure 7: Mean and standard deviation value of damage indicator *DI* for the respective load cycle.

The resulting curve stays somewhat around zero until cycle no. 7, where first damage initiation was identified by DIC (cf. Section 3.1). From this cycle onwards, the DI curve increases significantly. At the second damage initiation, identified at cycle no. 10, no significant change can be determined in the graph. For cycle no. 14 and 15, a slight decrease can be seen, however, as overlap damage continues to grow, the DI rises as well, until it reaches a final value of DI = 0.038 at cycle no. 28.

## 3.3  Damage indicator validation

The presented damage indicator is now validated by comparing it with the structural results, reported in detail in [5]. The tangential compliance from Section 3.1 is again shown in Figure 8, together with DI values for the respective load cycle. The DI values show a similar trend compared to the joint's tangential compliance. As already mentioned, the values increase at the first damage initiation and show no particular change at second damage initiation. After a decrease at cycle no. 14 and 15, the DI values increase monotonically until specimen failure.

In general, the proposed DI is capable of the evaluation of damage initiation and propagation at the hybrid joint's pinned SLS overlap.
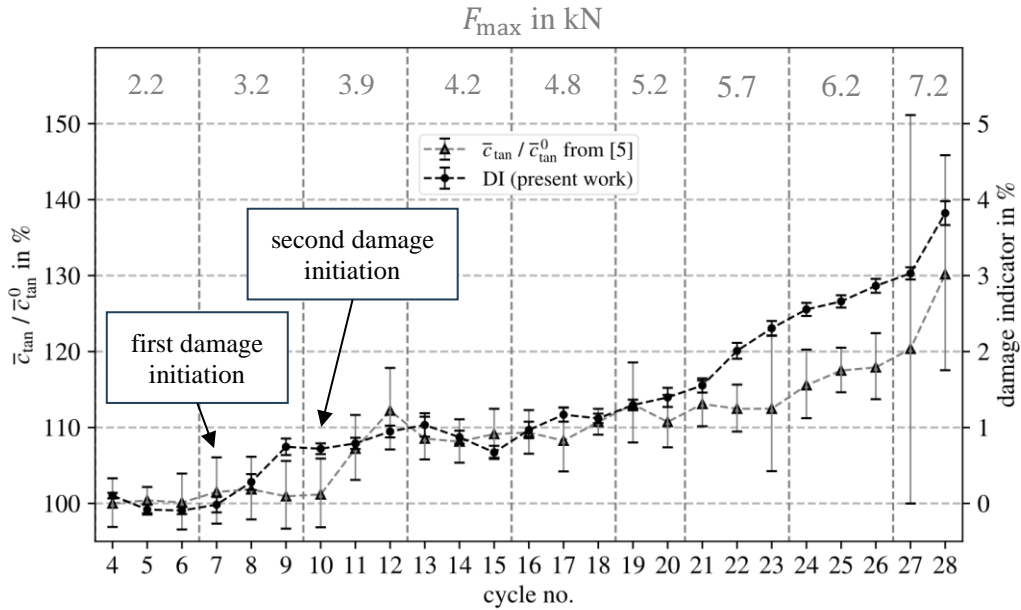


Figure 8: Comparison of the *DI* from the present investigation and results from [5].

In [5], the hybrid joint's electrically relevant regions (i.e., region with CFRP bulk material and region of the overlap) are investigated individually with their respective electrical potential and strain under unidirectional tensile loading. This was done to investigate the individual piezoresistive behavior when overlap damage occurs. It was found that overlap damage has no influence on the CFRP bulk material's behavior (this corresponds to the behavior of $R_1$). Consequently, in the present paper, the individual piezoresistive behavior does not need to be determined, since the electrical potential $U_1$ (CFRP bulk material) is not influenced by overlap damage. Therefore, the electrical potential $U_1$ is suitable as a reference measurement, which captures the global strain state of the specimen due to its unidirectional tensile loading. However, it is important to consider the characteristics of the SLS joint geometry under these specific loading conditions, as it results in a spatially inhomogeneous strain state at the overlap. For the investigation in [5], the evaluation and determination of gauge factors is elaborate and prone to influences of scattering DIC measurement data. This fact makes the present method more robust to influences such as noise in the optical measurements.

Consequently, to improve the present method even further, it is necessary to measure the voltage potentials $U_A$ and $U_B$ better. For this purpose, a complete 4-wire resistance measurement setup is suggested for future tests with pinned hybrid SLS specimen in order to minimize disturbing or falsifying influences, like for example, changing contact resistances of the electrical interconnections, etc.

## 4 CONCLUSIONS AND OUTLOOK

The present contribution proposes and demonstrates a new, simple DC ERM evaluation method for load-independent monitoring of damage initiation and propagation on pinned hybrid SLS joints comprised of titanium and epoxy resin-based CFRP adherends. For the examined joint, no costly conductivity-enhancing modifications are required to enable DC

ERM. A load-independent damage indicator is derived, which uses a simple electrical model to conclude from two measured electrical potentials on the non-reversible resistance change of pinned hybrid SLS joints. The damage indicator is discussed and validated by measurements at a specimen, which is subjected to quasi static, tension-tension loading and unloading cycles until rupture. The assumptions used to derive the proposed damage indicator are well supported, although the measurement data is highly scattered. A brief discussion of potential improvements in future electrical measurement setups is given. Damage initiation and propagation of the joint in the form of cracks at the overlap ends is the cause of detected non-reversible resistance change across the overlap, which is validated by the found degradation of the joint's tangential stiffness. Furthermore, the damage indicator is compared to the measured stiffness degradation, thereby showing its potential for evaluating damage propagation. Results are of similar quality as a damage indicator used in an earlier work but without the drawback of load-dependency.

Future research shall extend the proposed damage indicator to wider pinned hybrid SLS joints with multiple measurement points and paths and also consider 2-dimensional strain states.

## 5   ACKNOWLEDGEMENTS

## REFERENCES

[1]   S. Ucsnik, M. Scheerer, S. Zaremba, and D. H. Pahr, "Experimental investigation of a novel hybrid metal-composite joining technology," Composites Part A: Applied Science and Manufacturing 41 (2010), 369–374.
doi: 10.1016/j.compositesa.2009.11.003.

[2]   D. P. Graham, A. Rezai, D. Baker, P. A. Smith, and J. F. Watts, "The development and scalability of a high strength, damage tolerant, hybrid joining scheme for composite-metal structures," Composites Part A: Applied Science and Manufacturing 64 (2014), 11–24. doi: 10.1016/j.compositesa.2014.04.018.

[3]   A. Rytter, "Vibrational based inspection of civil engineering structures," Ph.D-Thesis, Aalborg University, Denmark (1993).

[4]   S. Nauman, "Piezoresistive Sensing Approaches for Structural Health Monitoring of Polymer Composites - A Review", Engineering 2 (2021), 197–226.
doi: 10.3390/eng2020013.

[5]   A. Dengg, C. Kralovec, and M. Schagerl, "Damage monitoring of pinned hybrid composite-titanium joints using direct current electrical resistance measurement". Manuscript submitted for publication.

[6]   ASTM D5868-01: Standard Test Method for Lap Shear Adhesion for Fiber Reinforced Plastic (FRP) Bonding (2014)

[7]   HexPly® 913 product data sheet, Hexcel Corporation

[8]   H. Peng, "Using laser etching to improve surface contact resistance of conductive fiber filler polymer composites," WO 02/19346 A1, 2001, World Intellectual Property Organization (2001)

[9]   M. Sutton, J.-J. Otreu, and H. Schreier, Image Correlation 682 for Shape, Motion and Deformation Measurements. Basic Concepts, Theory and Applications. Springer Science & Business Media, 2009, ISBN 978-0-387-78746-6

[10]   Vic-2D Reference Manual, Correlated Solutions Inc.

[11]   I. P. Nurprasetio, B. A. Budiman, A. A. Afwan, P. N. Halimah, S. T. Utami, and M. Aziz, "Nonlinear Piezoresistive Behavior of Plain-Woven Carbon Fiber Reinforced Polymer Composite Subjected to Tensile Loading", Applied Sciences, 10 (2020), 1366, doi: 10.3390/app10041366.